Geometric effects on convective coupling and interfacial structures in bilayer convection

D. Johnson and R. Narayanan
Department of Chemical Engineering, 227 Chemical Engineering Building, University of Florida, Gainesville, Florida 32611-6005
(Received 1 May 1997)

The effects of boundaries on bilayer convection in a cylinder with idealized boundary conditions are studied. Using as examples two bilayer systems, a plot of the Rayleigh number versus aspect ratio (radius-height) is calculated. For certain systems, the type of convection coupling, either thermal or viscous, will change as the width of the container changes, even as the height is fixed. Additionally, the interfacial structure is calculated to help identify the driving force for the convection. Sudden changes in the convection coupling and the dominant driving force of convection are found as the container radius increased. The oscillatory onset of convection and the possibility of oscillating nonlinear dynamics are also identified. [S1063-651X(97)03611-8]

PACS number(s): 47.27.Te

I. INTRODUCTION

Bilayer convection is an interesting transport process to study for reasons both theoretical and applied. Theoretically, bilayer convection is full of nonlinear dynamics with a wide range of parameters to study [1]. Some of the important applications of bilayer convection are as a model for convection in the earth's mantle [2] and liquid-encapsulated crystal growth.

In liquid-encapsulated crystal growth, the desired liquid to be solidified is placed in a cylindrical crucible. Another layer of liquid, called an encapsulant, is placed on top of the lower liquid, and this arrangement has a layer of inert gas placed on top of it. To solidify the lower liquid, the bottom of the cylinder is cooled, creating a temperature difference across the three fluid layers. This temperature difference then causes convection in the fluid layers by interfacial tension gradient and/or buoyancy forces. Convection is important in crystal growth as it will affect the quality of the crystal structure and the distribution of dopants in the crystal. As the lower liquid solidifies, the aspect ratio and the ratio of the fluid depths will continuously change.

When the aspect ratio of a convecting fluid changes, different flow patterns will occur at the onset of convection [3]. When the ratio of the fluid depths (upper depth divided by the lower depth) changes, the driving force for convection, and the type of convection, can change. For example, in small fluid depths, interfacial tension-driven convection (Marangoni convection) dominates. However, for deeper fluid layers, buoyancy-driven convection (Rayleigh convection) dominates.

In order to distinguish the various convective mechanisms, phrases such as ''convection initiating in one layer or another'' are introduced. Clearly, in a mathematical sense, there is only a single condition for the onset of convection, and this onset must occur simultaneously in both layers. The notion of convection ''initiating'' in one layer or another is ultimately a physical one, and is perhaps best explained qualitatively. To understand this statement in the context of convection with liquid bilayers, it is simpler to consider only Rayleigh convection, and therefore assume that the Marangoni effect is absent unless otherwise noted. Convection is said to initiate in one of the layers of a bilayer system, say the lower one, when the motion in that layer is dominant at the onset. Moreover, the onset of flow in the ''initiating'' layer is more or less independent of the adjacent layer that plays the role of a passive medium conducting heat away, and often responds by being dragged by the active layer. The magnitude of the velocities in the responding layer is usually much smaller than in the active layer in which convection is initiated.

To understand the various convective mechanisms, consider Fig. 1. Suppose that convection initiates in the lower layer. The upper layer responds by being dragged, generating

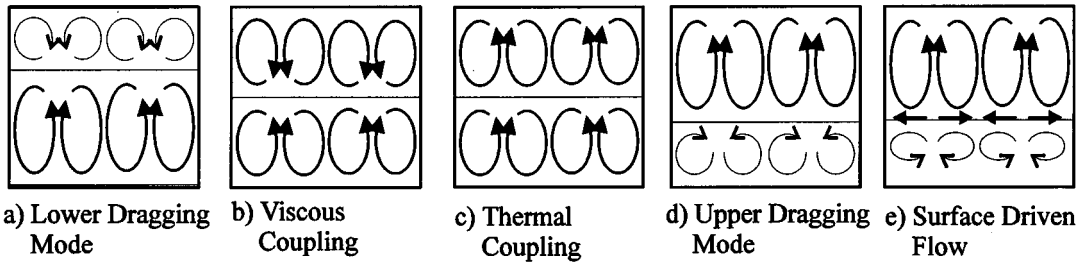

FIG. 1. Schematic of the different types of convection coupling. From the lower dragging mode to the upper dragging mode, the buoyancy force in the upper layer is increased and the dragging exerted by the lower layer decreases. Pure thermal coupling with surface-driven flow is caused by the upper fluid buoyantly convecting and simultaneously inducing surface tension- or buoyancy-driven convection in the lower layer, near the interface.

counter-rotating rolls near the interface. Hot fluid flows up in the lower layer and down in the upper layer. The upper layer is not buoyant enough, and moves by a combination of viscous drag and the Marangoni effect, whenever the latter is present. This is seen in Fig. 1(a). When the depth of the upper layer increases, so also does the effect of buoyancy on it. One of two things can happen. The first possibility is that both layers become ''viscously coupled.'' Buoyancy effects become comparable in both layers at convective onset, and the rolls counter-rotate in the two fluids, as depicted in Fig. 1(b). However, this is not all. The interface becomes an isotherm, and consequently the temperature perturbations on the base state switch sign there. This creates a ''zero perturbed isotherm'' immediately after onset of flow from the quiescent base state. This is the only way that hot fluid can rise in both layers near the interface. If the zero-perturbed isotherm were to occur in the domain in either layer, but close to the interface, one can then say that both fluids are ''nearly viscously coupled.'' For example, when the zero-perturbed isotherm occurs in the lower layer near the interface, it simply means that buoyancy-driven convection is slightly more dominant in the upper layer with some buoyancy-driven convection in the lower layer. In fact, Marangoni convection, whenever present, discourages this mode of operation [4], provided the interfacial tension decreases as temperature increases. The second possibility is ''thermal coupling,'' where the rolls are corotating. Here hot, rising fluid from the lower layer causes hot fluid to flow up in the upper layer. The vertical component of velocity and the temperature perturbations have the same sign in each fluid layer near the interface. Strictly speaking, the transverse components of velocity should be zero at the interface, although thermal coupling is sometimes loosely referred to as the case when a small roll develops in one of the layers in order to satisfy the no-slip condition at the interface.

As the buoyancy continues to increase in the upper layer, convection initiates in only the upper layer, and the lower layer is viscously dragged [Fig. 1(d)]. The last figure [Fig. 1(e)] is an example of what may be called ''pure thermal coupling with surface-driven flow.'' This typically occurs in a liquid-gas system, where buoyancy initiates in the upper gas layer, simultaneously sending thermal signature to the interface and generating either Marangoni or buoyancy convection in the lower layer [5]. Note that the convection in the lower layer is now generated purely by horizontal temperature gradients at the interface and not by viscous drag.

To determine each of the five convection-coupling modes experimentally, it would be necessary to monitor both the fluid direction and the isotherms of both fluid layers. This can be done using, for example, particle tracers to monitor the fluid flow and interferometry to measure the isotherms. Both of these methods are needed, for example, to distinguish between the lower dragging flow and the viscously coupled flow. The flow direction in each layer is the same, so particle tracking on its own could not distinguish the flow. However, the isotherms between the two cases are different. That is, hot upper layer fluid flows downward in the lower dragging mode, and cold upper layer fluid flows downward in the viscously coupled flow. To distinguish between the upper dragging mode and the surface-driven convection, one could look at the fluid flow direction. For fluids whose interfacial tension increases with an increase in temperature, the fluid flow direction in each layer will be the same as the upper dragging mode. In this situation, it may be difficult to determine which is the predominant driving force for flow in the lower layer. In fact, the two mechanisms would reinforce one another. However, when the upper fluid is a gas, then natural convection in the gas layer will not generate enough shear to give the upper dragging mode at the onset of convection.

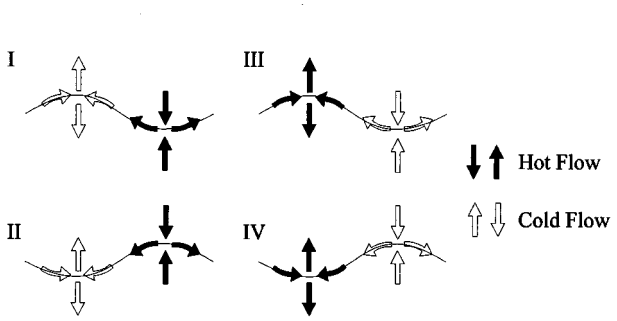

FIG. 2. The four possible interfacial structures at a fluid-fluid interface. Each structure can give information about the driving force of the convection.

Another indicator of what is occurring in bilayer convection can be inferred from the fluid-fluid interface instead of the bulk convection. In the paper by Zhao *et al.* [6], four different interfacial structures were identified for any given convecting bilayer with a deflecting interface. Each of these structures depends upon whether fluid was flowing into or away from the trough or the crest, and whether the fluid was hotter or cooler at the trough or the crest of the interface. Hot fluid flowing into a trough defines the first interfacial structure. The second interfacial structure has hot fluid flowing into a crest. The third structure has hot fluid flowing away from a crest and the fourth structure has hot fluid flowing away from a trough. Each of these four scenarios is given in Fig. 2.

One of the important factors to consider in interfacial structures is the direction of the flow along the interface. As interfacial tension is usually inversely proportional to temperature, at cooler regions of the interface, the interfacial tension will be higher and will pull on the interface. Where the interface is hotter, the interfacial tension will be lower causing the fluid to move away from warmer regions. Another important factor is the direction of the flow into or away from a crest or a trough. One reason the interface deflects is due to bulk convection, caused by buoyancy effects pushing against the interface. Consider two fluids whose dynamic viscosities are equal. If buoyancy-driven convection occurs mostly in the lower layer, then the fluid will flow up from the lower layer into a crest. If the fluid flows down from the top layer into a trough, then one would argue that buoyancy-driven convection occurs mostly in the upper fluid. The second reason an interface deflects is due to the pushing and pulling caused by variations in the interfacial tension.

In each of the four cases, the interfacial structure can be used to indicate the driving force of the convection. In the first interfacial structure, the dominating driving force is in-

TABLE I. Table of dimensionless numbers.

Name	Symbol	Equation
Rayleigh number	Ra	$g\alpha_1\Delta T_1 d_1^3/\kappa_1\nu_1$
Marangoni number	Ma	$\sigma_1\Delta T_1 d_1/\kappa_1\mu_1$
Prandtl number	Pr	ν_1/κ_1
Crispation number	C	$\mu_1\kappa_1/\sigma_0 d_1$
Weber number	G	$(\rho_1-\rho_2)gd_1^2/\sigma_0$
Ratio of thermal expansions	α	α_2/α_1
Ratio of fluid depths	l	d_2/d_1
Ratio of thermal conductivities	k	k_2/k_1
Ratio of thermal diffusivities	κ	κ_2/κ_1
Ratio of densities	ρ	ρ_2/ρ_1
Ratio of dynamic viscosities	μ	μ_2/μ_1

terfacial tension-driven convection. This is seen as the cold fluid, with the higher interfacial tension pulling the interfacial fluid into the crest. In the second interfacial structure, buoyancy drives convection in the lower phase. The hot, rising fluid pushes the interface upwards. As the fluid moves along the interface, it cools and eventually sinks back down. The third interfacial structure is dominated by buoyancy-driven convection in the upper phase, or by interfacial tension-driven convection where the interfacial tension increases with respect to temperature. The fourth interfacial structure occurs in the rare instance where the lower fluid has a positive thermal-expansion coefficient. In other words, the density increases with an increase in the temperature, causing the cooler, lower fluid to flow up into a crest. The paper by Zhao *et al.* gives more details of each interfacial structure.

In Sec. II, the mathematical model used to describe bilayer convection in a laterally unbounded geometry is given. The connection between the results obtained in such a geometry and to those in a bounded circular cylinder with restrictive boundary conditions is made. This section is then followed by a detailed discussion of the observations with an explanation of the physics of multilayer convection as a function of the aspect ratio.

II. MODEL

The mathematical model used to study and determine each of these systems is found in the paper by Ferm and Wollkind [7]. In this model, a system of two fluid layers is bounded on the top of the upper fluid, and the bottom of the lower fluid by rigid, conducting plates; see Fig. 3. The interface between the lower and upper fluid is allowed to deflect. The model is bounded in the vertical direction by rigid plates, and is infinite in the horizontal direction. The density and interfacial tension for both fluids are assumed to be a linear function of the temperature. The symbol σ will be used for interfacial tension and its variation with respect to temperature is $\sigma_1=-\partial\sigma/\partial T|_{T_{\rm ref}}$, evaluated at the reference temperature. The length, velocity, time, and pressure are scaled with d_1, κ_1/d_1, d_1^2/κ_1, and $\mu_1\kappa_1/d_1^2$, respectively, where, d_1, κ_1, and μ_1 are the depth, thermal diffusivity, and dynamic viscosity of the lower fluid. Additional parameters are listed in Table I. Here, the subscript 1 denotes the lower fluid. A subscript 2 will denote the upper fluid. The temperature is scaled with respect to the temperature difference across the lower liquid layer.

The equations used in the Ferm and Wollkind model are the familiar steady-state Boussinesq equations. A linear stability analysis is subsequently performed on each equation. Each state variable, A is expanded in a perturbation series in ε, a quantity that represents the magnitude of convection. The perturbation series takes the form

$$A=A^{(0)}+\varepsilon A^{[1]}+\varepsilon^2 A^{[2]}+\cdots,$$

where $A^{[1]}=dA/d\varepsilon|_{\varepsilon=0}$ and $A^{(0)}$ is the quiescent, conductive state with a flat interface. The interface position, $z=\eta$, is clearly a function of ε, and at the interface

$$A^{[1]}=A^{(1)}+\frac{\partial A^{(0)}}{\partial z}\,\eta_1,$$

where $A^{(1)}=\partial A/\partial\varepsilon|_{\varepsilon=0}$ and $\eta_1=\partial\eta/\partial\varepsilon|_{\varepsilon=0}$. If A is a domain variable, $A^{[1]}=A^{(1)}$. Further expansion into normal modes yields

$$A^{(1)}(z)=\overline{A(z)}e^{i\omega x}e^{qt},$$

Using the above with $q=0$, the quantities with the overbars are dropped. The domain equations in the lower phase are

$$\begin{aligned}
DW_1+i\omega U_1&=0,\\
(D^2-\omega^2)U_1-i\omega\Pi_1&=0,\\
(D^2-\omega^2)W_1-D\Pi_1+\mathrm{Ra}\Theta_1&=0,\\
(D^2-\omega^2)\Theta_1+W_1&=0.
\end{aligned}\tag{1}$$

The first of these equations is obtained from continuity, while the next two equations are a result of linearizing the momentum equation and the last equation is the energy equation. Likewise, the domain equations in the upper phase are

$$\begin{aligned}
DW_2+i\omega U_2&=0,\\
\frac{\mu}{\rho}(D^2-\omega^2)U_2-\frac{i\omega}{\rho}\Pi_2&=0,\\
\frac{\mu}{\rho}(D^2-\omega^2)W_2-\frac{1}{\rho}D\Pi_2+\alpha\,\mathrm{Ra}\Theta_2&=0,\\
\kappa(D^2-\omega^2)\Theta_2+\frac{1}{k}W_2&=0.
\end{aligned}\tag{2}$$

The 13 boundary conditions are

$$W_2=W_1=0 \quad \text{at } z=0,$$

$$DW_2=DW_1 \quad \text{at } z=0,$$

$$\Pi_2-\Pi_1+\left(\frac{G+\omega^2}{C}\right)\eta_1+2(DW_1-\mu DW_2)=0 \quad \text{at } z=0,$$

$$(D^2+\omega^2)W_1-\mu(D^2+\omega^2)W_2=\omega^2\,\mathrm{Ma}(\eta_1-\Theta_1)$$

$$\text{at } z=0,$$

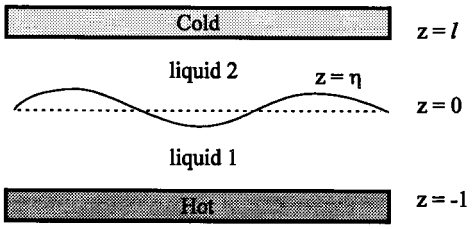

FIG. 3. Schematic of the bilayer model.

$$kD\Theta_2 = D\Theta_1 \quad \text{at } z=0$$

$$\Theta_1 = \Theta_2 + \eta_1(1-1/k) \quad \text{at } z=0,$$

$$DW_1 = W_1 = \Theta_1 = 0 \quad \text{at } z=-1,$$

$$DW_2 = W_2 = \Theta_2 = 0 \quad \text{at } z=l, \tag{3}$$

where $D \equiv d/dz$. A table of all dimensionless numbers is given in Table I.

The dependent variables in each phase are W_i for the vertical component of velocity, Θ_i for the temperature, Π_i for the pressure, and η_i for the surface deflection term. In further calculations, the horizontal components of velocity in both fluid layers are eliminated by substituting the equation of continuity.

A Chebyshev spectral tau method [8] was used to solve the system of equations (1)–(3). This method easily incorporates the complicated boundary conditions and provides the accuracy needed using only a few number of terms. After applying this spectral method, the ordinary differential equations reduce to an eigenvalue problem. The eigenvalue is the Rayleigh number. Each Rayleigh number can be solved for a range of wave numbers, ω. The result is a plot of the Rayleigh number versus the wave number, shown in Fig. 4.

In a technique exemplified by the papers of Rosenblat and co-workers [9–11], the Rayleigh number versus wave number plot can be ''unfolded'' into a Rayleigh number versus aspect ratio plot. The way this process works is by assuming that the container, in which the two fluids reside, has peculiar boundary conditions. For a cylinder, these boundary conditions are insulating sidewalls, and vanishing vertical and tangential components of vorticity. For a rectangular geometry, the boundary conditions are stress-free and insulating sidewalls. However, in this paper only cylindrical geometries will be considered. When these boundary conditions are assumed for a three-dimensional cylindrical geometry, a separation of variables technique can be used to solve for the independent variables, W_1, W_2, Θ_1, Θ_2, Π_1, and Π_2, where

$$W_i = W_i(z) J_m(\lambda_{m,n} r)\cos(m\theta),$$

$$\Theta_1 = \Theta_i(z) J_m(\lambda_{m,n} r)\cos(m\theta) \quad \text{for } i=1,2 \tag{4}$$

$m=0,1,2,\ldots$ is the azimuthal wave number, $n=0,1,2,\ldots$ is the radial wave number, and $J_m(\lambda_{m,n} r)$ are the Bessel functions. The value $\lambda_{m,n} = s_{m,n}/\gamma$ is determined from the requirement that $J'_m(\lambda_{m,n}\gamma)=0$, where $s_{m,n}$ are the zeros of the derivative of the Bessel's function, and γ is the aspect ratio. It can be shown that the functions $W_1(z)$, $W_2(z)$, $\Theta_1(z)$, $\Theta_2(z)$, $\Pi_1(z)$, and $\Pi_2(z)$ are the same functions solved in the unbounded model. Therefore, the simpler unbounded model can be used to find qualitative features of the flow field in a cylinder. Upon further observation, a relationship between the wave number ω and the aspect ratio γ is found to be

$$\gamma = \frac{s_{m,n}}{\omega}. \tag{5}$$

Therefore, for each wave number at a given azimuthal and radial mode, there is a corresponding aspect ratio, γ. (This will be shown in Fig. 7.)

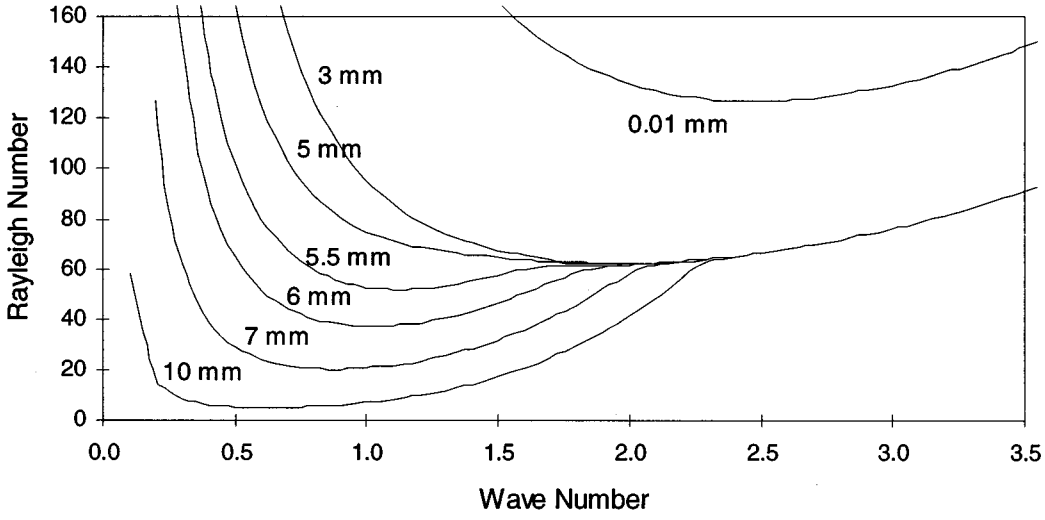

FIG. 4. Plot of the Rayleigh number of silicone oil vs the wave number for various air heights. As the air height increases, the critical wave number decreases.

TABLE II. Possible combinations of the ratio of the temperature perturbations to surface deflection, and the ratio of the derivative of the vertical component of velocity to the surface deflections. The four different combinations predict different behavior in the bulk fluid.

	$\Theta_1^{[1]}(0)/\eta$	$DW_1(0)/\eta$
Case I	negative	positive
Case II	positive	negative
Case III	positive	positive
Case IV	negative	negative

To determine whether the bilayer convection is thermally or viscously coupled, one need only look at the vertical component of velocity and the temperature profiles [5,12]. To find out which interfacial structure is present, two different ratios need to be calculated. The first ratio is the perturbed temperature evaluated at the interface, $\Theta^{[1]}(0)$, divided by the interfacial deflection η_1. The second ratio is the derivative of the velocity evaluated at the interface, $DW_1(0)$, divided by the surface deflection. If the first ratio is positive, then the fluid must be warmer at a crest. If the second ratio is positive, then the fluid must flow away from a crest; see Table II. The perturbed temperature $\Theta^{[1]}$ at $z=0$ is actually $\Theta^{(1)}+\eta_1$, and so the first ratio is $(\Theta_1+\eta_1)/\eta_1$, where the superscript (1) is dropped, and the subscript, 1 refers to the lower phase, and gives the values of each ratio for each of the four possible interfacial structures.

III. DISCUSSION

In this section, the convection-coupling mechanism and the interfacial structure will be studied for two different bilayer systems. In each case, the fluid depths are changed to observe different interfacial structures or different convection-coupling mechanisms near the minimum of the Rayleigh number versus wave number plots. When this occurs and the plot is subsequently unfolded, the interfacial structure and the convection-coupling mechanism will change as the aspect ratio of the container increases. Because of the large number of dimensionless groups (Table I) the main ideas in this paper are exemplified by calculations for two bilayer systems. These are the silicone oil-air system and the glycerol-silicone oil system. Their properties are shown in Table III. Note the different signs of the interfacial tension gradient σ_1 in each of the bilayer systems.

Changes in convection coupling

The first system considered is the popular silicone oil and air system. As was noted in Ref. [5], when the air layer is large, convection initiates in the air. This convection then creates a temperature difference across the liquid interface, simultaneously causing interfacial tension-induced convection. Continuing this reasoning, various depths of silicone oil and air were considered where convection is equally likely to initiate in either the lower or the upper layer.

As an example, a depth of 2 mm of silicone oil, for a variety of air heights, was chosen. For each air height, a plot of the Rayleigh number versus wave number was calculated

TABLE III. Thermophysical properties of the two bilayer systems used in the calculations: (1) silicone oil and air, and (2) glycerol and silicone oil.

	Bilayer system 1		Bilayer system 2	
Property (units)	Silicone oil	Air	Glycerol	Silicone oil
ρ_i (g/cm^3)	0.968	0.0012	1.26	0.97
α_i (10^4 °C^{-1})	9.6	33.3	4.9	9.45
k_i (10^{-4} erg/cm s °C)	1.59	0.262	2.94	1.6
κ_i (10^{-3} cm^2/s)	1.10	182	0.89	1.16
ν_i (Stokes)	0.692	0.157	7.45	4.99
σ_0 (dyn/cm)	20.9		25	
σ_1 (dyn/cm °C)	0.05		−0.13	

(Fig. 4). For small air heights (0.01 mm) the critical wave number is 2.55, and gradually decreases as the air height increases. For example, the critical wave number for a 3-mm air height is 2.00. The critical wave number is the value of the wave number at the minimum of the Rayleigh number versus the wave-number curve, for a fixed air height. At an air height greater than 5 mm, the critical wave number drastically shifts to lower values. This occurs due to the dominant convection in the air layer. As the air height increases, the buoyancy effect in the air layer increases, and eventually becomes greater than the buoyancy effect in the silicone oil.

Before the effect of the aspect ratio on the convection mechanism is explained, it would be instructive to make additional comments on these mechanisms. To do this efficiently, consider Fig. 1. As noted earlier, Fig. 1(a) is the situation where the convection is dominant in the lower layer, and the upper layer responds by being dragged. An example of this is shown in Fig. 5(a) for the silicone oil-air system. Observe that the sign of the velocity switches from the lower to upper layer, and that the maximum of the lower layer velocity is generally much greater than the maximum of the upper layer velocity in magnitude. The corresponding situation in Fig. 1(b) is depicted in Fig. 5(b). Here the magnitudes of the lower and upper velocities are of comparable order, and the velocity and the temperature change sign from the lower to upper layers. Additionally, hot fluid flowing up toward the interface in the lower layer is combined with hot fluid flowing down in the upper layer at the interface. This appears to contradict our view taken earlier that the upper fluid is also buoyant. On further inspection of the numbers that generate the temperature perturbation plot, an isotherm $\Theta(z)=0$ is observed in the domain of the upper fluid very near the interface and to the right of the vertical dotted line, which represents the unperturbed interface. In other words, hot fluid does flow up in the upper layer but not at the interface. Here the bilayer is nearly viscously coupled.

Figure 1(c) can be nearly depicted by Fig. 5(c). Observe that the velocities in both the upper and lower layers show comparable minima, and a small counter-roll has developed in the air layer to preserve the no-slip condition between the fluids. It is possible to obtain a situation where no counter-roll develops in the upper layer. In this situation, this would be called pure thermal coupling, as no motion in either layer is generated by viscous drag. In other words, it is possible to obtain a structure where the fluid depths are such that the thermal coupling in perfect, corotating rolls are obtained. In

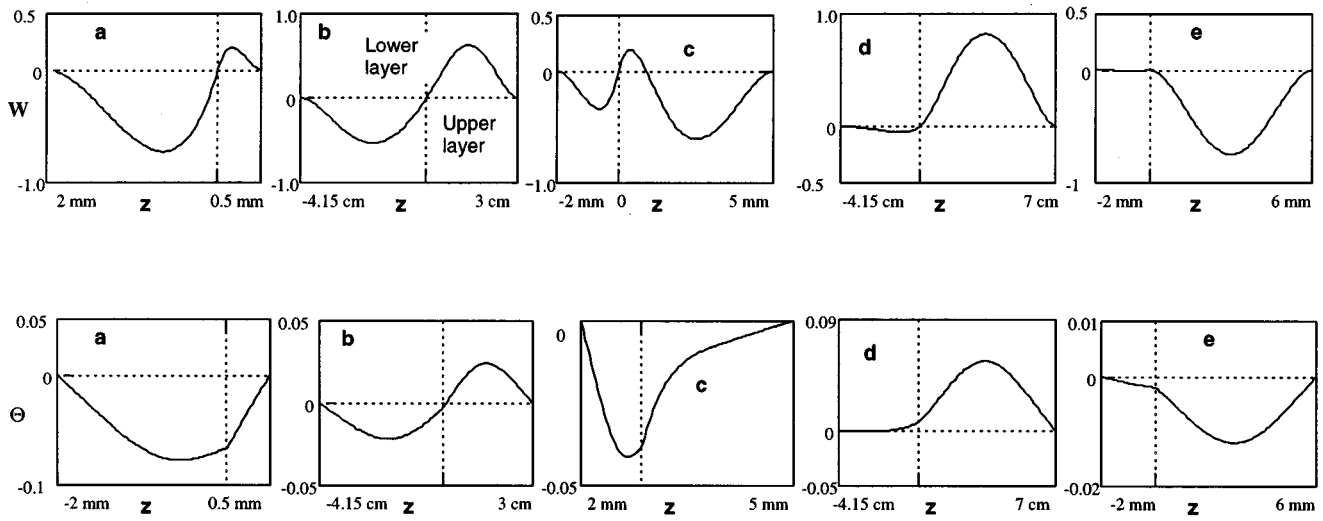

FIG. 5. Plots of the vertical component of velocity (top row) and the temperature perturbations (bottom row). (a) 2 mm of silicone oil and 5 mm of air, $\omega=2.0$. (b) 4.15 cm of glycerol and 3 cm of silicone oil, $\omega=3.8$. (c) 2 mm of silicone oil and 5 mm of air, $\omega=1.9$. (d) 4.15 cm of glycerol and 7 cm of silicone oil, $\omega=3.8$. In (e), 2 mm of silicone oil and 6 mm of air, $\omega=1.0$. Calculations were done for a laterally unbounded geometry. The vertical dotted line represents the unperturbed interface position.

such a situation, the transverse components of velocity perturbations at the interface are zero. This can be seen later in this paper with liquid bilayers [see Fig. 11(a) as an example] Fig. 1(d) cannot be depicted in a silicone oil-air system, because the air does not drag the silicone oil due to the very small ratio of dynamic viscosities. However, the calculations using glycerol-silicone oil system show this dragging effect well [Fig. 5(d)]. This situation is qualitatively the reverse of Fig. 5(a). The last convection mechanism, Fig. 1(e), is seen in calculations using silicone oil-air [Fig. 5(e)]. Notice that within the scale of the plot, the lower velocity is nearly zero. A closer look at the actual numbers indicates that the velocity in the lower fluid has the same sign as the velocity in the upper fluid, and is less than 1% of the maximum velocity in the upper fluid.

Returning to the task of relating the aspect ratio to convection mechanisms, the vertical component of velocity for both fluids is plotted for two different wave numbers, for a 5-mm air height (Fig. 6). At a wave number of $\omega=1.9$, Fig. 6(a) shows mostly a thermal coupling of the silicone oil and air. For a larger wave number of $\omega=2.7$, Fig. 6(b) shows mostly dragging of the air by the silicone oil. This feature is most enhanced after the plots are unfolded.

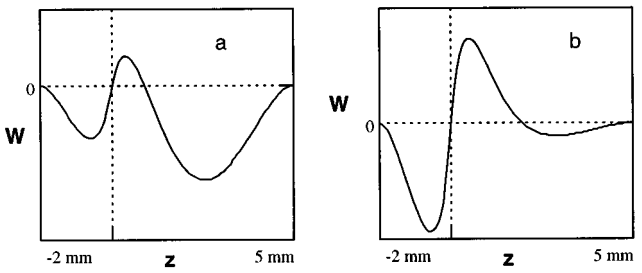

FIG. 6. Plot of the vertical component of velocity for a wave number of 1.9 (a) and 2.7 (b). The depth of the silicone oil was 2 mm, and the depth of the air was 5 mm. In (a), $\omega=1.9$, and the air is mostly thermally coupled. In (b), $\omega=2.9$, and the air is mostly viscously coupled.

The next step is to unfold Fig. 4 using Eq. (5). The result is shown in Fig. 7, for various azimuthal and radial modes. Each azimuthal and radial mode determines a different flow pattern at the onset of convection. The same plots in Fig. 6 now represent the vertical component of velocity for various aspect ratios. For example, the wave number of 2.7 converts to an aspect ratio of 0.68 for the unicellular $(m=1,n=1)$ flow. The wave number of 1.9 converts to an aspect ratio of 1.6 for a bimodal flow pattern $(m=2,n=1)$.

What does this exercise explain? It shows that for cylinders (as well as rectangular geometries), the type of convection-coupling mechanism can change as the aspect ratio increases. There are two ways the aspect ratio of the liquid can change, either changing the radius or the height. In Fig. 7, the height of the silicone oil is fixed at 2 mm. Therefore, Fig. 7 corresponds to a situation where the radius is being changed. The next question that can be raised is the following: why does changing the radius of the cylinder affect the type of convection?

The change in the convection coupling as the aspect ratio increases can best be explained by analyzing the Rayleigh number versus aspect ratio plots for each fluid layer. The Rayleigh number for each fluid is defined as

$$\mathrm{Ra}_1=\frac{\alpha_1 g\Delta T_1 d_1^3}{\kappa_1\nu_1}, \tag{6}$$

$$\mathrm{Ra}_2=\frac{\alpha_2 g\Delta T_2 d_2^3}{\kappa_2\nu_2}. \tag{7}$$

The temperature difference in each phase, ΔT_1 or ΔT_2, is calculated from the linear conduction state just prior to the onset of convection. As the width of the container increases, the aspect ratios of each layer increase. However, the energy

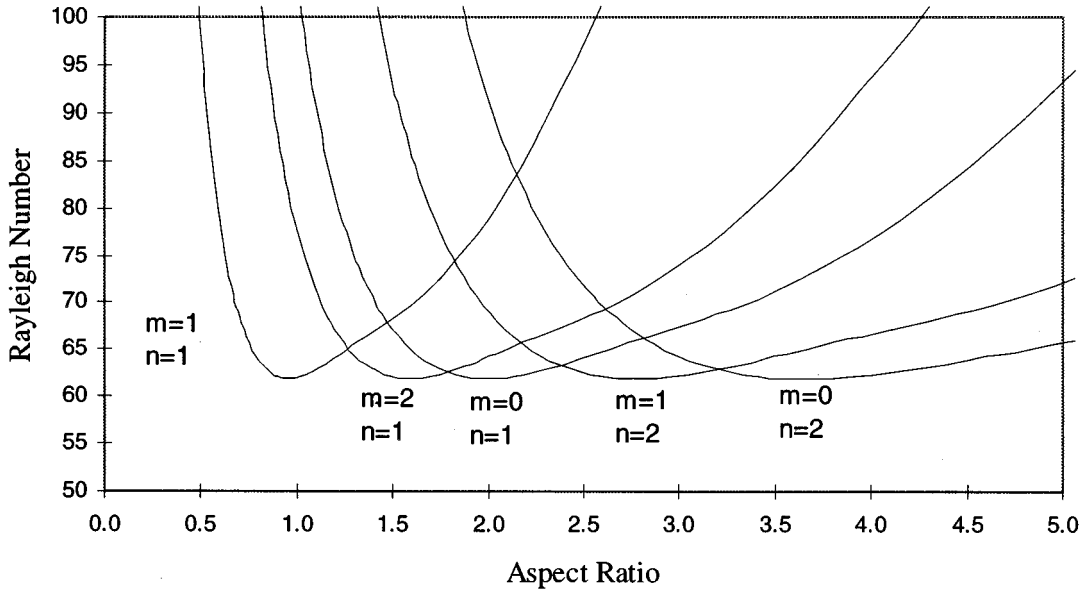

FIG. 7. Plot of the Rayleigh number of the silicone oil vs the cylindrical aspect ratio. This plot was generated from Fig. 4 and the wave number to aspect ratio conversion formula [Eq. (5)]. A depth of 2 mm of silicone oil and a 5-mm air height was assumed.

required to convect each layer changes with the aspect ratio, and this could either increase for both, decrease for both or increase for one and decrease for the other. This ambiguity results because the critical Rayleigh number is a nonmonotonic function of the aspect ratio. In other words, increasing the aspect ratio can easily cause the convection mechanism to change—generating a situation like Fig. 1(b) for one aspect ratio and Fig. 1(c) for another. Other mechanisms [Figs. 1(a), 1(d), and 1(e)] are also possible, and depend on the particular bilayer system being studied.

Changes in the interfacial structure

In the next set of calculations, a silicone oil-air bilayer system was also chosen. In this exercise, the Rayleigh number versus the wave number plots are generated for 6 mm of air and various depths of the silicone oil: 2.5, 3.0, and 3.5 mm. In Fig. 8, the solid lines denote a case I interfacial structure, and the dotted lines denote a case II interfacial structure. As was discussed in the Sec. I, case I indicates interfacial tension gradient-driven convection, and case II indicates buoyancy-driven convection in the lower layer.

For 3.0 mm of silicone oil, the interfacial structure changes from case I to case II at the critical wave number. When the silicone oil layer increases to 3.5 mm, the buoyancy-driven case II interfacial structure becomes more unstable. When the silicone oil height decreases to 2.5 mm, the interfacial tension-driven case I interfacial structure becomes more unstable. This is in qualitative agreement with

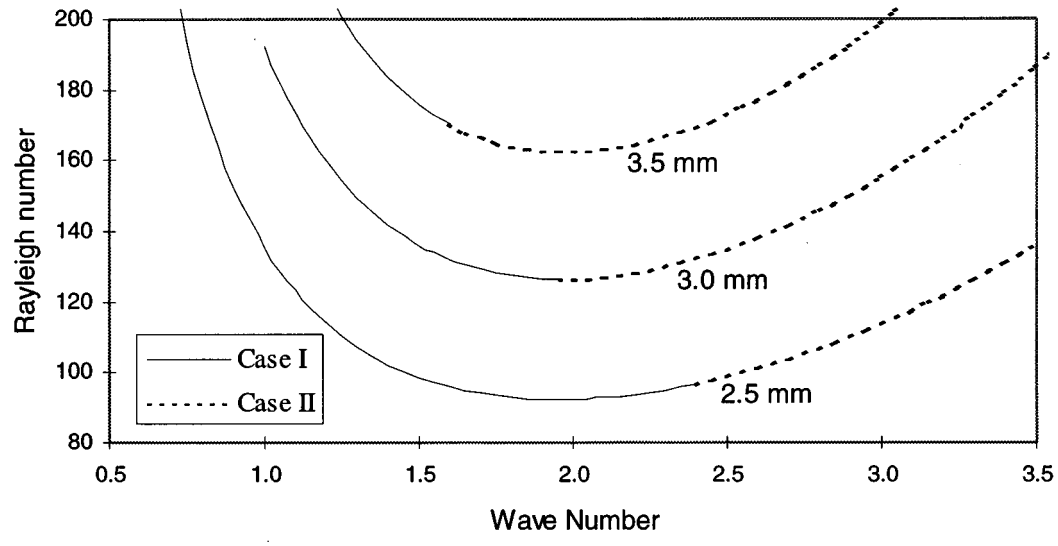

FIG. 8. Plot of the Rayleigh number of the silicone oil vs the wave number for three different depths of the silicone oil. The solid lines denote a case I interfacial structure, and the dotted lines denote a case II interfacial structure. The air height is 6 mm.

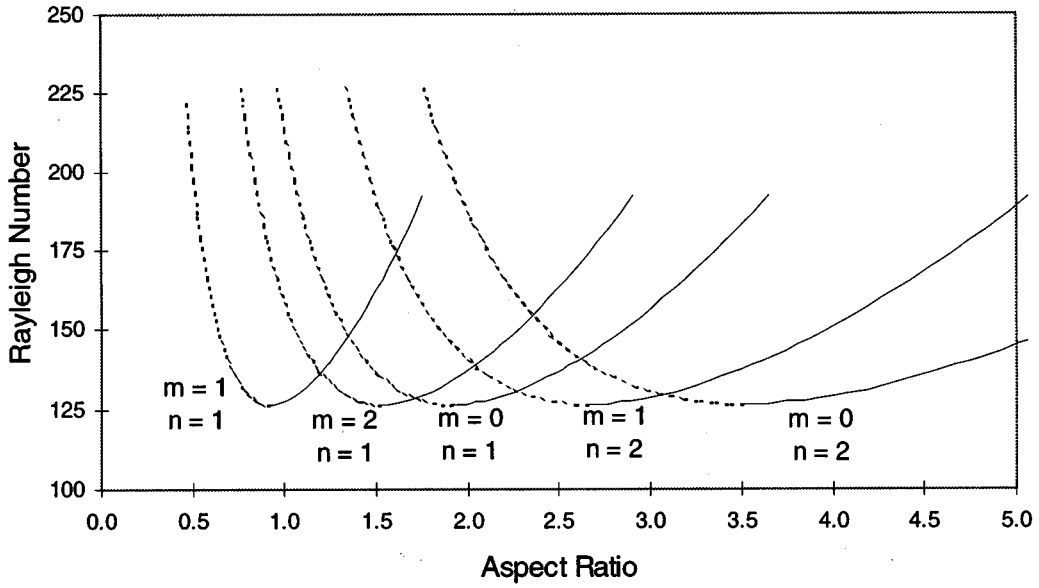

FIG. 9. Plot of the Rayleigh number of the silicone oil vs the aspect ratio. Solid lines denote a case I interfacial structure. Dotted lines denote a case II interfacial structure.

the physics. As the silicone oil layer increases, buoyancy forces become more dominant than interfacial tension gradient forces. As the silicone oil layer decreases, interfacial tension gradient forces become more dominant.

When Fig. 8 is unfolded, the dominating driving force for convection can change as the aspect ratio increases, and this is depicted in Fig. 9. This is most pronounced at codimension-2 points, where two flow patterns coexist. Typically, the change from one interfacial structure to the next is quite gradual. The surface deflections slowly flatten as the interfacial structure switches from case II to case I. This can be seen around an aspect ratio of 0.9. At codimension-2 points, though, the switch from one interfacial structure to the next can be abrupt. That is, on one side of the codimension-2 point, the fluid is buoyancy driven, with one spatial pattern, then switches to a interfacial tension gradient-driven flow on the other side of the codimension-two point, with a different spatial pattern. For example, this can be seen at codimension-2 points with aspect ratios of 1.2 and 1.7.

Other observations in convection coupling and interfacial structure

In the last example the liquid-liquid bilayer glycerol-silicone oil is examined. The thermophysical properties, which are listed in Table III, are taken from Ref. [13]. In this system, switching between different convection mechanism and three different interfacial structures can be seen.

Figure 10 again gives a plot of the Rayleigh number versus wave number for a glycerol-silicone oil bilayer. Glyc-

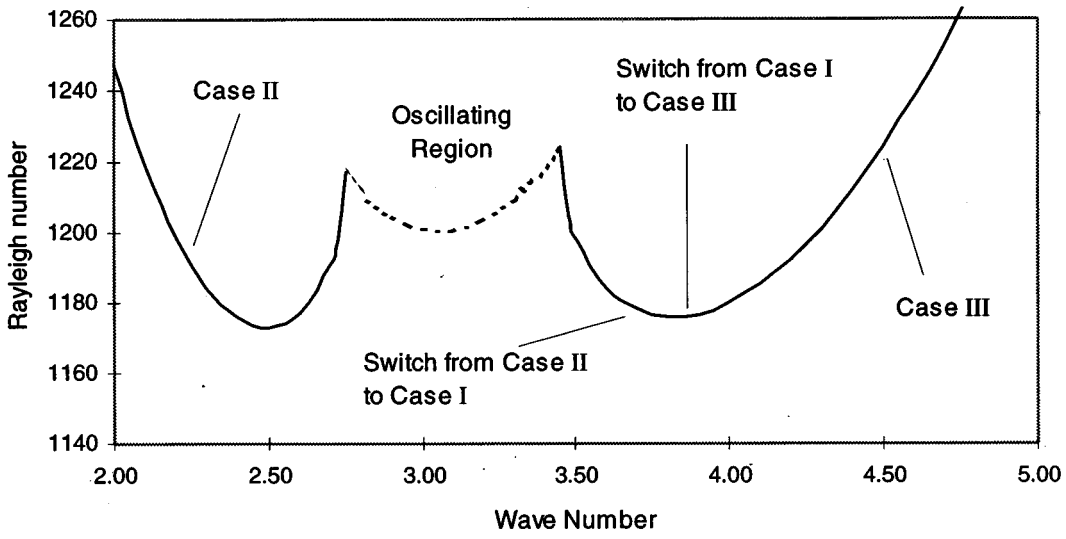

FIG. 10. Plot of the Rayleigh number of the glycerol vs the wave number. A 4.15-cm height of glycerol and a height of 3.0-cm silicone oil were assumed.

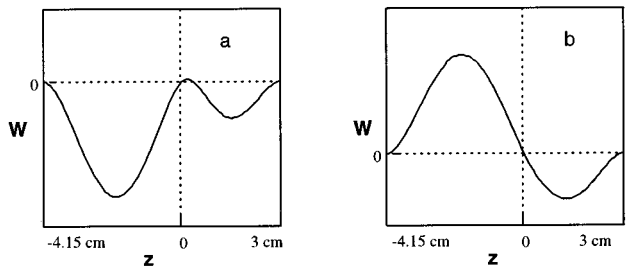

FIG. 11. Plot of the vertical components of velocity for 4.15 cm of glycerol and 3.0 cm of silicone oil. In (a), the two fluids are thermally coupled, with a small counter roll in the upper layer, $\omega = 2.7$. In (b), the two fluids are viscously coupled $\omega = 3.5$. The vertical dotted line is the unperturbed interface.

erol, which has the larger density, lies below the layer of silicone oil. The height of the glycerol is 4.15 cm, and the height of the silicone oil is 3.0 cm. For the calculations performed, only steady and no Hopf bifurcations were analyzed. The Rayleigh number was calculated, and when the imaginary part of the Rayleigh number became nonzero, it was inferred that the onset of convection was oscillatory. While for real values of the Rayleigh number the numbers are correct, for complex values, the real part of the Rayleigh number has no physical interpretation. The dotted lines in Figs. 10 and 12 are regions where oscillations occur. This does not change the qualitative discussion given below, and therefore it was felt that a full search for the Hopf bifurcations were unnecessary.

A plot of the vertical component of velocity for $\omega = 2.7$ and 3.5 are given in Fig. 11. For $\omega = 2.7$, the convection is nearly thermal coupled, with a small counter-roll in the upper fluid. For $\omega = 3.5$, the convection is viscously coupled. Indeed, as indicated by previous researchers, the oscillations in Fig. 10 are due to a competition between the thermal and viscous coupling.

The call-outs in Fig. 10 denote wave numbers at which the interfacial structure changes. For a wave number less than 3.8, the interfacial structure is case II. Between $\omega = 3.8$ and 3.9, the interfacial structure is case I. For wave numbers greater than $\omega = 3.9$, the interfacial structure is case III. Here also the interfacial structure changes near the wave numbers where an oscillatory onset of convection occurs.

Both the interfacial structures and the convection-coupling can be used to describe what is occurring in the two liquids. For wave numbers smaller than the oscillatory region, the two fluids are nearly thermally coupled and the interfacial structure is a case II. As was described earlier, a case II interfacial structure denotes buoyancy-driven convection occurring in the lower layer. The hot plumes of the lower layer rise up and drive convection in the upper liquid, creating a thermally coupled bilayer, with a small counter-roll. For wave numbers much larger than the oscillatory region ($\omega > 3.9$), the convection is viscously coupled, and the interfacial structure is a case III flow structure. For a case III interfacial structure, buoyancy-driven convection occurs mostly in the upper layer. The cold, sinking fluid in the upper layer pushes down and depresses the interface. In this study, the interfacial structure seems to indicate that viscous coupling occurs when the upper fluid ''initiates'' convection, causing the lower fluid to flow and convect in a gearlike manner.

What seems somewhat peculiar is the case II interfacial structure at wave numbers between $\omega = 3.4$ and 3.8, while the two fluids are viscously coupled. However, this can be explained by the differences in the dynamic viscosities of the two fluids. The dynamic viscosity of glycerol is about twice that of the dynamic viscosity of the silicone oil. Even though convection may begin to initiate in the silicone oil, the silicone oil must overcome the higher dynamic viscosity of the glycerol. Only when the silicone oil convection is much more vigorous does it begin to deflect the interface down to give a case III interfacial structure. The case I interfacial structure is a transitional structure between cases II and III.

Unfolding Fig. 10 gives an extremely interesting and complicated plot of the Rayleigh number versus the aspect ratio (see Fig. 12). The dark lines represent viscous coupling, the thinner lines represent thermal coupling, and the dotted lines represent the oscillatory onset of convection. Four different flow patterns are given.

At different aspect ratios, the flow can be either thermally coupled, viscously coupled, or oscillating between these two states, at the onset of convection. Some of the most interesting aspect ratios, however, occur at the codimension 2 points. For example, the codimension-2 point around an aspect ratio of 0.8 goes from a thermally coupled unicellular flow ($m = 1, n = 1$), to a viscously coupled bimodal flow ($m = 2, n = 1$). There is a high probability that at these codimension-2 points, nonlinear interactions will be very dynamic. In the paper by Johnson and Narayanan [14], a dynamic switching between an axisymmetric $m = 0$ flow and a bimodal $m = 2$ flow was experimentally found in the slightly supercritical region, near a codimension-2 point. In that system, only a single layer of silicone oil was used. Andereck Colovas, and Degen [15] found oscillations between viscous coupling and thermal coupling in a silicone oil-flourinert system. When these two phenomena are combined, a highly oscillatory state in the supercritical region is quite possible. Even more interesting dynamics may occur at codimension-2 points such as the 1.1 aspect ratio. Here a codimension-2 point is close to an oscillating bimodal flow and an oscillating axisymmetric flow. Fujimura and Renardy [16] studied convection at a codimension-2 point between Hopf bifurcations and steady bifurcations. Their paper was able to reveal the wealth of dynamics that can occur in these systems.

One important point must be considered before these results are compared with experiments. As pointed out in the papers by Dauby and co-workers [17,18] and in the paper of Zaman and Narayanan [19], the order in which the modes appear as the aspect ratio is increased, is different for vorticity-free sidewalls and no-slip sidewalls. Additionally, the Rayleigh numbers for the unfolded plots are not the same as those in a bounded calculation, especially for smaller aspect ratios. While the differences between vorticity-free sidewalls and no-slip sidewalls are not to be ignored, the effects of aspect ratios on convection mechanisms and interfacial structures with realistic sidewall conditions are expected to be qualitatively similar to the vorticity-free case.

IV. SUMMARY AND CONCLUSIONS

Calculations performed for bilayer convection in laterally unbounded geometries give a qualitative picture of the dif-

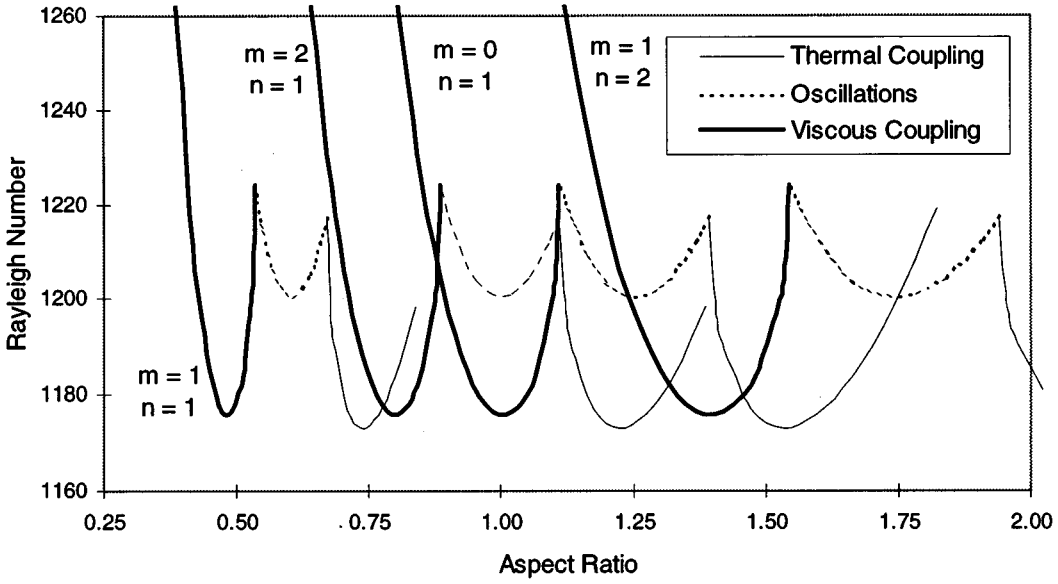

FIG. 12. Plot of the Rayleigh number of the glycerol vs the aspect ratio. The plot is generated from Fig. 10 and Eq. (5). As the aspect ratio changes, the convection switches from viscous coupling, to oscillatory flow, and to thermal coupling.

ferent ways in which convection can occur in a bounded cylinder. These different types of bilayer convection depend upon the layer in which the convection is the most dominant. The types of convection also depend upon how the layer that did not initiate convection responds to the layer that did initiate convection.

The hierarchy of convection mechanisms has been explained both by looking at interfacial structures and also by considering the perturbed temperature and velocity profiles through the fluid layers. Specific examples of silicone oil-air and glycerol-silicone oil have been used to exemplify the arguments made. Having done this, the mechanisms of the onset of convection in a bounded right circular cylinder was explained. Because the difficulty of the computations is determined by the sidewall conditions, it was assumed that the vertical and tangential components of vorticity vanished at the vertical sidewalls. This assumption allows the results of the unbounded case and the qualitative features as a function of the aspect ratio to be determined. It was observed that the aspect ratio did indeed affect the nature of the onset of convection. As the depths of the fluids were assumed constant, it was apparent that the change in radius could affect the physics of the flow and flow structures. This unusual result is explained by the observation that a change in the radius changes the aspect ratios of both fluid layers, and the energy required for each layer to convect changes differently with aspect ratio because of differing thermophysical properties. Moreover, the onset of oscillations and sudden pattern changes at codimension-two points were observed.

All of this will have an impact on future studies where bilayer convection is of importance. For example, a nonlinear analysis of the bilayer systems should determine which codimension-2 points give interesting oscillating behavior. The effects of bounded geometry on bilayer convection should lead to many exciting experiments. Experiments, where the onset of convection is unsteady and the Rayleigh numbers in each fluid layer are comparable, ought to show many of the phenomena discussed above.

The discovery of many of these oscillations will have practical applications in liquid-encapsulated crystal growth. As the lower liquid solidifies, the aspect ratio of the lower liquid and the depth ratios will change. Oscillatory convection ought to be seen when the lower liquid aspect ratio reaches a codimension-2 point, and when the liquid depth ratios are such that the buoyancy forces in each layer are equal. Oscillatory convection is of particular interest in crystal growth, as the fluctuating temperature continually melts, then solidifies, the crystal, creating defects in the crystal.

ACKNOWLEDGMENTS

The National Science Foundation (CTS 93-07819) and NASA (NGT 3-52320) are acknowledged for funding and support.

[1] P. Colinet and J. C. Legros, Phys. Fluids **6**, 2631 (1994).

[2] F. M. Richter and C. E. Johnson, J. Geophys. Res. **79**, 1635 (1974).

[3] E. L. Koschmieder and S. A. Prahl, J. Fluid Mech. **215**, 571 (1990).

[4] R. W. Zeren and W. C. Reynolds, J. Fluid Mech. **53**, 305 (1972).

[5] D. Johnson, R. Narayanan, and P. C. Dauby, J. Fluid Mech. (to be published).

[6] A. X. Zhao, C. Wagner, R. Narayanan, and R. Friedrich, Proc.

R. Soc. London, Ser. A **451**, 487 (1995).
[7] E. N. Ferm and D. J. Wollkind, J. Non-Equilib. Thermodyn. **7**, 169 (1982).
[8] C. Canuto, M. Y. Hussaini, A. Quarteroni, and T. A. Zang, *Spectral Methods in Fluid Dynamics* (Springer-Verlag, Berlin, 1988).
[9] S. Rosenblat, J. Fluid Mech. **122**, 395 (1982).
[10] S. Rosenblat, S. H. Davis, and G. M. Homsy, J. Fluid Mech. **120**, 91 (1982).
[11] S. Rosenblat, S. H. Davis, and G. M. Homsy, J. Fluid Mech. **120**, 123 (1982).
[12] S. Rasenat, F. H. Busse, and I. Rehberg, J. Fluid Mech. **199**, 519 (1989).
[13] P. Cardin, H. C. Nataf, and P. Dewost, J. Phys. (France) II **1**, 599 (1991).
[14] D. Johnson and R. Narayanan, Phys. Rev. E **54**, R3102 (1996).
[15] C. D. Anderek, P. W. Colovas, and M. M. Degen, *Advances in Multi-Fluid Flows* (SIAM, Philadelphia, 1996) Vol. 3.
[16] K. Fujimura and Y. Y. Renardy, Physica D **85**, 25 (1995).
[17] P. Dauby and G. Lebon, J. Fluid Mech. **329**, 25 (1996).
[18] P. Dauby, G. Lebon, and E. Bouhy, Phys. Rev. E **56**, 520 (1997).
[19] A. Zaman and R. Narayanan, J. Colloid Interface Sci. **179**, 151 (1996).